Acta Cryst. (1979). A35, 1001–1009

Direct Phasing of Electron Diffraction Data from Organic Crystals: The Effect of *n*-Beam Dynamical Scattering

BY DOUGLAS L. DORSET

Medical Foundation of Buffalo, Inc., 73 High Street, Buffalo, New York 14203, USA

BING K. JAP

Department of Physics, University of Alberta, Edmonton, Alberta, T6G 2J1, Canada

AND MING-HSIU HO AND ROBERT M. GLAESER

Division of Medical Physics, Donner Laboratory, University of California, Berkeley, CA 94720, USA

(*Received* 21 *March* 1979; *accepted* 10 *July* 1979)

Abstract

The conditions under which direct phasing methods might be used to determine the crystallographic phases from electron diffraction intensity data are investigated through numerical calculations for two organic crystals. The Cowley–Moodie multislice formulation of dynamical diffraction theory is used to calculate the diffraction intensity data for various crystal thicknesses, at electron energies of 100 keV and 1·0 MeV. The direct phasing method is found to give generally correct phases up to a crystal thickness of about 75 Å at 100 keV. The use of higher electron energy (*i.e.* 1·0 MeV) produces a significant improvement in the success of the direct phasing approach at crystal thicknesses greater than 75 Å.

Introduction

Very few organic or light-atom crystal structures have been determined *ab initio* from electron diffraction intensity data, despite claims that these data satisfy the kinematical approximation (Vainshtein, 1964). In fact, most reported 'determinations' have utilized a previous X-ray crystal structure analysis to supply the phasing model. For the few cases where crystal structures were determined from the diffraction data alone, trial and error methods were most commonly invoked to derive the phasing model. Patterson methods have been seldom used and in at least one such case (Boudeulle, 1975) the derived structure was shown to be incorrect by later X-ray and neutron diffraction analysis (Heger, Klein, Pintschovius & Kahlert, 1978).

The use of direct phasing methods, which are based upon probabilistic estimates of phase invariants (Hauptman, 1972), has been reported only once for electron diffraction data (Dorset & Hauptman, 1976). On the other hand, this methodology has revolutionized X-ray crystal structure analysis on 'small molecules' (*i.e.* structures – centric or noncentric – with less than 100 non-hydrogen atoms in the asymmetric unit).

It is important to determine the conditions under which direct phasing techniques may be successfully applied to electron diffraction data from organic crystals. Many such data sets from single, thin plate crystals exist only as two-dimensional zonal projections. The most commonly found noncentric space groups for organic compounds (Nowacki, Matsumoto & Edenharter, 1967) are (in decreasing order): $P2_12_12_1$, $P2_1$ and $P2_12_12$. Of these, only $P2_1$ has (two) noncentric projections. The others reduce to centric phasing problems $(0,\pi)$ for zonal projections, thus simplifying the phasing for these limited data sets.

It is our aim to extend the exploration of direct phasing methodology for organic crystal structure analysis from electron diffraction intensity data by considering the effect of *n*-beam dynamical scattering on this phasing. The assumption of crystal perfection for *n*-beam calculations does not accurately represent the conditions under which experimental data are often obtained, since organic crystals are subject to many deformations and other defects (Dorset, 1977, 1978). However, the assumption of crystal perfection should provide a useful guideline, or approximation, to the experimental conditions under which direct phasing may safely be employed.

Model crystal structures

Two previously determined organic crystal structures were used to generate *n*-beam dynamical diffraction amplitudes for subsequent direct phasing procedures. These are: anhydrous cytosine (Barker & Marsh, 1964)

0567-7394/79/061001-09$01.00

which is represented in Fig. 1 and has eight non-hydrogen atoms per asymmetric unit; and disodium 4-oxypyrimidine-2-sulfinate hexahydrate (Slettin, 1969), here called 'DISOPS', which is shown in Fig. 2 and has 16 'heavy' atoms per asymmetric unit. At the outset it should be mentioned that the projections considered in the direct phasing process contain the largest unit-cell axes. This is an artifice from the standpoint of normal crystal growth for aromatic compounds (Jensen, 1970) but is justified by experimental electron diffraction and imaging studies of larger aromatics (Uyeda, Kobayashi, Suito, Harada & Watanabe, 1972; Murata, Fryer & Baird, 1976) where similar crystal projections are deposited by epitaxial growth onto a substrate.

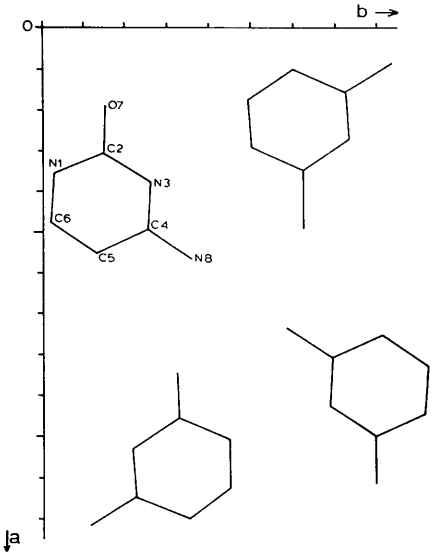

Fig. 1. Crystal structure of anhydrous cytosine after Barker & Marsh (1964), (001) projection; a = 13·041, b = 9·494, c = 3·815 Å, space group $P2_12_12_1$, zonal plane group: *pgg*. In this drawing, the origin is shifted to two-fold axis of *pgg* to allow only phases $0, \pi$.

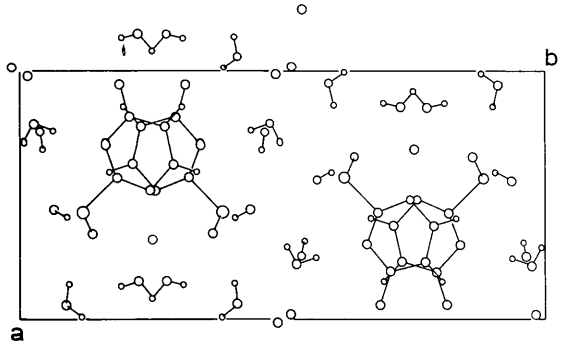

Fig. 2. Crystal structure of disodium 4-oxypyrimidine-2-sulfinate hexahydrate (DISOPS) after Slettin (1969), (001) projection; a = 9·2988, b = 20·2529, c = 6·9460 Å, space group *Pbcm*, zonal plane group: *pgm*.

It also should be mentioned that such two-dimensional data, as used in this paper, minimize a restriction imposed by crystal bending, *i.e.* the crystal projection which gives diffracted data *least* perturbed by bend effects is that with the smallest unit-cell axis parallel to the incident beam (see Cowley, 1961; Dorset, 1978). Bent crystals with long cell axes parallel to the incident beam can cause an apparent shortening of the diffraction coherence length to a value less than the unit-cell length. This experimentally observed effect may make the actual use of three-dimensional data very difficult.

Structure-factor calculations in this study utilized the electron scattering-factor tables of Doyle & Turner (1968). No attempt was made to simulate partially-charged ion pairs in the DISOPS structure. Standard crystallographic programs (structure factor, Fourier maps) used here are part of the system of programs written for the PDP 11/45 computer at the Medical Foundation of Buffalo, Inc. by Dr Charles Weeks *et al.*

n-Beam dynamical calculations

The diffracted-wave function in the multislice dynamical formulation can be described by the following recursive relationship (Cowley & Moodie, 1957; Jap & Glaeser, 1979),

$$F_n(\mathbf{h}) = \{F_{n-1}(\mathbf{h}) * Q(\mathbf{h})\} \times \exp[-i\pi\lambda\Delta z_n(h^2/a^2 + k^2/b^2)],$$

$$Q(\mathbf{h}) = \mathsf{F}\left\{\exp\left[-\frac{i}{\hbar v}\int_{z_{n-1}}^{z_n} eV(x,y,z)\,\mathrm{d}z\right]\right\},$$

where $F_n(\mathbf{h})$ is the diffracted wave function that would be obtained after passing through a sequence of n slices, the symbol $*$ denotes the convolution product, Δz_n is the thickness of the nth slice, a and b are crystal constants (orthorhombic lattice), F is the Fourier transform operator, $eV(x,y,z)$ is the crystal potential energy, $\hbar$ is Planck's constant divided by 2π, and v is the electron relativistic velocity.

The numbers of reflections included in the initial calculation of the dynamical diffracted wave function are 949 and 943, respectively, for cytosine and DISOPS. The widest-angle data for use in the direct phasing procedure were essentially at the resolution of the input data for the n-beam dynamical calculations for cytosine (0·65 Å) and DISOPS (0·80 Å). The slice thickness used is one unit cell thick along the shortest crystal axis. For cytosine this is 3·815 Å, while for DISOPS it is 6·946 Å. The effect of thermal motion of the atoms was ignored in the kinematic as well as the dynamical calculations. More complete details of the multislice calculations, including a comparison of the kinematic and 'weak phase object' approximations, are given by Jap & Glaeser (1980).

Calculation of normalized diffraction amplitudes and their statistical distribution

n-Beam dynamical diffraction amplitudes for the various crystal thicknesses and the two accelerating voltages were scaled to the calculated kinematical structure factors by demanding $\sum |F_{kin}| = \sum |F_{dyn}|$. Note that the appellation 'kinematical' is not used in its strictest sense in this paper. As used, it denotes diffraction amplitudes calculated with known atomic positions and the Doyle–Turner scattering form-factor tables in a fashion analogous to X-ray calculations. However, the effect of Ewald-sphere curvature is not included in this calculation for a zonal data set, and the method of calculation therefore corresponds to what is often called the weak phase object approximation. The agreement between the sets of normalized dynamical diffracted-wave moduli and the 'kinematical' moduli is expressed in Table 1 as an R factor.

Table 1. *Summary of input and derived parameters for direct phasing*

Compound	Data set	Accelerating voltage	Crystal thickness in Å (slices)	Number of reflections with $\|E\| > 1.0$	R factor*
Cytosine	1	100 kV	7·6 (2)	68	0·07
	2		76 (20)	63	0·71
	3		300 (80)	78	0·96
	4	1000 kV	7·6 (2)	66	0·06
	5		76 (20)	64	0·23
	6		300 (80)	71	0·51
	7		610 (160)	79	0·66
DISOPS	1	100 kV	14 (2)	69	0·07
	2		69 (10)	71	0·57
	3		280 (40)	77	0·97
	4		350 (50)	86	0·87
	5	1000 kV	14 (2)	72	0·05
	6		69 (10)	71	0·15
	7		280 (40)	84	0·68
	8		560 (80)	82	0·68
	9		690 (100)	84	0·74

*$R = \sum ||F_{kin}| - k|F_{dyn}|| / \sum |F_{kin}|$. Data scaled such that $\sum |F_{kin}| = \sum |F_{dyn}|$.

The scaled dynamical diffraction amplitudes were treated subsequently as 'observed' data for direct phasing programs. The first step was to calculate normalized structure factors ($|E|$'s) from these 'observed' magnitudes ($|F|$'s), *i.e.*

$$E_{\mathbf{h}}^2 = |F(\mathbf{h})|^2 \Big/ \left[\varepsilon \sum_{i=1}^{N} f_i^2(\mathbf{h})\right].$$

Here ε is a multiplicity factor, N is the number of atoms in the unit cell, and $f_i(\mathbf{h})$ is the (electron) scattering form factor for atom i at $(\sin\theta/\lambda)_{\mathbf{h}}$. These $|E|$ values are used in subsequent direct phasing programs to allow the estimate of phase-invariant cosines. In the triple phase invariants used to phase the dynamical data, only $|E|$'s greater than 1·0 were considered such that the probability of any estimate of phase cosine would be close to 1·0. The number of zonal data above this limit is given for each compound in Table 1.

Another useful statistic is a test for centrosymmetric distributions of data which is based on theoretical estimates for $|E|$'s (Karle, Dragonette & Brenner, 1965). A comparison of these experimental distributions of $|E|$'s with the theoretical values is shown in Tables 2 and 3 for the two crystal structures. Both

Table 2. *Cytosine statistical distribution of normalized structure factors* ($|E|$'s)

	Theoretical (centric)	Theoretical (acentric)	Data sets 1	2	3	4	5	6	7
$\langle\|E\|\rangle$	0·798	0·886	0·777	0·782	0·794	0·778	0·763	0·837	0·836
$\langle\|E\|^2\rangle$	1·000	1·000	1·000	1·000	1·000	1·000	1·000	1·000	1·000
$\langle\|\|E\|^2 - 1\|\rangle$	0·968	0·736	1·003	1·012	0·997	1·005	1·064	0·821	0·876
$\|E\|$, % > 1·0	32·00	37·00	27·533	26·652	29·515	28·414	26·432	32·819	32·747
$\|E\|$, % > 2·0	5·00	1·80	4·626	4·626	4·626	4·185	6·167	4·626	3·077
$\|E\|$, % > 3·0	0·30	0·01	0·881	0·881	1·322	0·881	1·762	0·000	0·879

Table 3. *Statistical distribution of normalized structure factors* ($|E|$'s) *for disodium 4-oxypyrimidine-2-sulfinate hexahydrate* (*DISOPS*)

	Theoretical (centric)	Theoretical (acentric)	Data sets 1	2	3	4	5	6	7	8	9
$\langle\|E\|\rangle$	0·798	0·886	0·815	0·829	0·838	0·879	0·815	0·851	0·879	0·863	0·866
$\langle\|E\|^2\rangle$	1·000	1·000	1·000	1·000	1·000	1·000	1·000	1·000	1·000	1·000	1·000
$\langle\|\|E\|^2 - 1\|\rangle$	0·968	0·736	0·936	0·898	0·816	0·759	0·935	0·868	0·748	0·801	0·795
$\|E\|$, % > 1·0	32·00	37·00	29·759	29·978	32·385	32·543	31·788	30·769	35·667	34·573	36·703
$\|E\|$, % > 2·0	5·00	1·80	3·501	4·814	0·438	1·751	3·091	3·077	2·626	2·188	2·857
$\|E\|$, % > 3·0	0·30	0·01	0·000	0·000	0·438	0·000	0·000	0·000	0·000	0·438	0·000

crystal structures have relevant zonal projections which are centric. All cytosine data sets (Table 2) satisfy the criterion for centrosymmetry. However, with increasing crystal thickness (and hence enhancement of n-beam interactions), the DISOPS data become more and more acentric in their distribution.

Direct phasing procedure

Unlike the previous application of direct phasing to electron diffraction data where phase cosines for both three-phase ('triple') and four-phase ('quartet') invariants in space group $P\bar{1}$ were estimated, an automated phasing program *QTAN* (Langs & DeTitta, 1975) was utilized to obtain the phases of the reflections with $|E| \geq 1{\cdot}0$. *QTAN* estimates the cosine values of triple phase invariants based on the magnitude of a parameter α. This is related to the familiar $A_{\mathbf{h},\mathbf{k}} = 2|E_{\mathbf{h}}E_{\mathbf{k}}E_{\mathbf{h}-\mathbf{k}}|/N^{1/2}$ for the invariant $\Phi_{\mathbf{h},\mathbf{k}} = \varphi_{\mathbf{k}} + \varphi_{\mathbf{h}-\mathbf{k}} - \varphi_{\mathbf{h}}$ by

$$\alpha_{\mathbf{h}_{\text{est}}} = \left\{ \sum_{\mathbf{k}} A^2_{\mathbf{h},\mathbf{k}} + 2 \sum_{\mathbf{k}\neq\mathbf{k}'} \sum A_{\mathbf{h},\mathbf{k}} A_{\mathbf{h},\mathbf{k}'} \times \frac{I_1(A_{\mathbf{h},\mathbf{k}}) I_1(A_{\mathbf{h},\mathbf{k}'})}{I_0(A_{\mathbf{h},\mathbf{k}}) I_0(A_{\mathbf{h},\mathbf{k}'})} \right\}^{1/2},$$

where I_0 and I_1 are Bessel functions of imaginary argument. For centric space groups, the phases of the reflections $\mathbf{h}$ are estimated by evaluating the $\alpha_{\mathbf{h}}$ weighted vector sum of all triple invariants which contain this phase term.

As usual, a limited number of phases can be defined arbitrarily by definition of origin. For a zonal projection of a primitive centric unit cell, this number is two, with Miller indices of parity such that, individually or added together, they are not two even integers (*e.g.* see Stout & Jensen, 1968). These chosen phases, when inserted into the triple invariants, will generally define a small number of other phases. To access the other phases for the centric zone a few other phases can be inserted as 'ambiguities'; thus phase sets are generated with all permutations and combinations of these ambiguously defined phases. If two are needed to access the whole set of $|E|$'s, then four possible solutions are generated based on these ambiguities having values $(0,0)$, $(0,\pi)$, $(\pi,0)$ and (π,π).

The use of phase ambiguities necessitates the use of some figure of merit to determine which phase set is most probable. This becomes most important when many ambiguities are needed, giving more possible solutions than are easily evaluated by Fourier maps. In this study, two principal figures of merit were monitored for indicating the actual structural solution. The first, NQEST, is defined (DeTitta, Edmonds, Langs & Hauptman, 1975):

$$\text{NQEST} = \sum_{\mathbf{h},\mathbf{k},\mathbf{l}}^{N} B \cos(\varphi_{\mathbf{h}} + \varphi_{\mathbf{k}} + \varphi_{\mathbf{l}} + \varphi_{\mathbf{m}}) \Big/ \sum_{\mathbf{h},\mathbf{k},\mathbf{l}}^{N} B,$$

where $B = (2/N)|E_{\mathbf{h}}E_{\mathbf{k}}E_{\mathbf{l}}E_{\mathbf{m}}|$. This quantity is evaluated over all so-called 'negative' four-phase invariants (quartets) for which 'main' $|E|$'s ($|E_{\mathbf{h}}|$, $|E_{\mathbf{k}}|$, $|E_{\mathbf{l}}|$ and $|E_{\mathbf{m}}|$) are large and 'cross term' $|E|$'s ($|E_{\mathbf{h}+\mathbf{k}}|$, $|E_{\mathbf{h}+\mathbf{l}}|$ and $|E_{\mathbf{h}+\mathbf{m}}|$) are small. It has been shown for X-ray crystal structures that the more negative NQEST is, the more likely the phase solution will be correct (DeTitta, Edmonds, Langs & Hauptman, 1975). In the course of the direct phasing procedure, all possible negative quartets are generated for $B > B_{\text{min}}$; $|E_{\mathbf{h}+\mathbf{k}}|$, $|E_{\mathbf{h}+\mathbf{l}}|$ and $|E_{\mathbf{h}+\mathbf{m}}| \leq |E_{\text{cross}}|$; and $|E_{\mathbf{h}}|$, $|E_{\mathbf{k}}|$, $|E_{\mathbf{l}}|$, $|E_{\mathbf{m}}| \geq |E_{\text{min}}|$. For our work these three limits were, respectively: 0·30, 0·60 and 1·00.

The second figure of merit is a residual, often termed R_{Karle}, which is based on a Sayre product average over a limited region of reciprocal space (Karle & Karle, 1966). The quantity R_{Karle} is defined as

$$R_{\text{Karle}} = \sum_{\mathbf{k}_r} \big| |E_{\mathbf{h}}|_{\text{obs}} - |E_{\mathbf{h}}|_{\text{calc}} \big| \Big/ \sum_{\mathbf{k}_r} |E_{\mathbf{h}}|_{\text{obs}},$$

where

$$|E_{\mathbf{h}}|^2_{\text{calc}} = \sigma_2^{3/2}\sigma_2^{-1}[\langle |E_{\mathbf{k}}E_{\mathbf{h}-\mathbf{k}}| \cos(\varphi_{\mathbf{k}} + \varphi_{\mathbf{h}-\mathbf{k}})\rangle^2_{\mathbf{k}_r} + \langle |E_{\mathbf{k}}E_{\mathbf{h}-\mathbf{k}}| \sin(\varphi_{\mathbf{k}} + \varphi_{\mathbf{h}-\mathbf{k}})\rangle^2_{\mathbf{k}_r}].$$

In this expression the $|E_{\mathbf{h}}|_{\text{obs}}$ are obtained from the experiment. The quantities σ_n are defined as

$$\sigma_n = \sum_{j=1}^{N} Z_j^n,$$

where Z_j is the atomic scattering factor for atom j at $\sin\theta/\lambda = 0$. In practice, the summation over $\mathbf{k}_r$ involves only those vectors for which $|E_{\mathbf{h}}| > 1$. A low value of R_{Karle} can be taken as evidence in support of the correctness of the phase set determined by the use of direct methods (Karle & Karle, 1966).

Results of direct phasing

The results of the direct phasing process for the two compounds are reviewed in Table 4 and represent the derived phase sets with the best agreement to the known phases. It is seen that the figures of merit are not infallible for the choice of the best phase set. However, a combined use of NQEST and R_{Karle} narrows the choice to (at most) two potential maps in these examples.

The best appraisal of the efficacy of direct phasing is obtained from inspection of the Fourier maps. Fourier maps calculated from F's were found to be clearer than

those calculated from E's. In five of the seven conditions tested for cytosine, the potential maps give a recognizable image of the molecule. Four of these maps are very well defined (Fig. 3*a*) with atoms well resolved and with positions corresponding to those derived from the X-ray crystal structure analysis. Another map (Fig. 3*b*) which is still recognizable as cytosine (100 kV, 76 Å thickness, data set No. 2) has some atoms which are spuriously placed and weighted. Other data sets with more phase errors give maps which cannot be identified (Fig. 3*c*).

Similar results are obtained with DISOPS. Four conditions produce maps in which all atoms of the structure can be found (Fig. 4*a*). Since this structure contains some atoms which, in projection, have nearly overlapping positions, their resolution is not very good on the map. However, the same thing would be found in a limited set of phased X-ray diffraction data. As more and more phase errors occur in the direct phasing, due to enhanced dynamical effects, the maps become less representative of the true crystal structure (Fig. 4*b*–*f*).

It should also be noted that the R factor does not have its conventional significance when one compares n-beam dynamical diffraction amplitudes with kinematical structure factors. In conventional use with X-ray or neutron data (for which the diffraction conforms to the kinematical model), the R factor indicates errors both in placement of atoms during the crystal structure solution and in the intensity data themselves (due to measurement error, 'extinction', absorption, *etc.*). For this study the positions of the atoms are known and the calculated data are therefore

Table 4. *Results of direct phasing*

Compound	Data set	Number of incorrect phases for $\|E\| > 1{\cdot}0$	Figures of merit for best set of phases NQEST	R_{Karle}	Is potential map recognizable?
Cytosine	1	0	−0·348	0·233	yes
	2	2	−0·146[a]	0·235	yes
	3	17	−0·539	0·269	no
	4	0	−0·342	0·239	yes
	5	0	−0·351	0·342[b]	yes
	6	1	−0·199[a]	0·422	yes
	7	13	0·024	0·422[b]	no
DISOPS	1	4	−0·296	0·366	yes
	2	3	−0·424	0·395	yes
	3	35	−0·013[a]	0·517[b]	no
	4	27	−0·605[a]	0·401	no
	5	1	−0·268	0·375	yes
	6	3	−0·468	0·332	yes
	7	17	0·031	0·492[b]	no
	8	27	−0·100[a]	0·439	no
	9	31	−0·088[a]	0·591[b]	no

Notes: (*a*) Not lowest NQEST.
(*b*) Not lowest R_{Karle}.

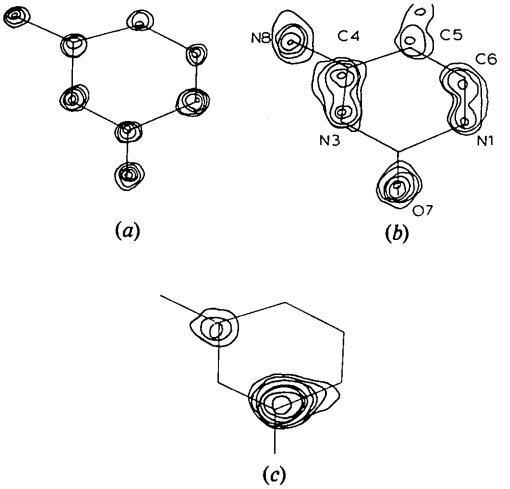

Fig. 3. Potential maps for cytosine after direct phasing (asymmetric unit only). (*a*) Successful solution map representative of: 100 kV, 7·6 Å thick (No. 1); 1000 kV, 7·6 Å thick (No. 4); 1000 kV, 76 Å thick (No. 5); 1000 kV, 300 Å thick (No. 6). (*b*) Distorted map with discernible molecule: 100 kV, 76 Å thick (No. 2). (*c*) Unrecognizable structure: 100 kV, 300 Å thick (No. 3).

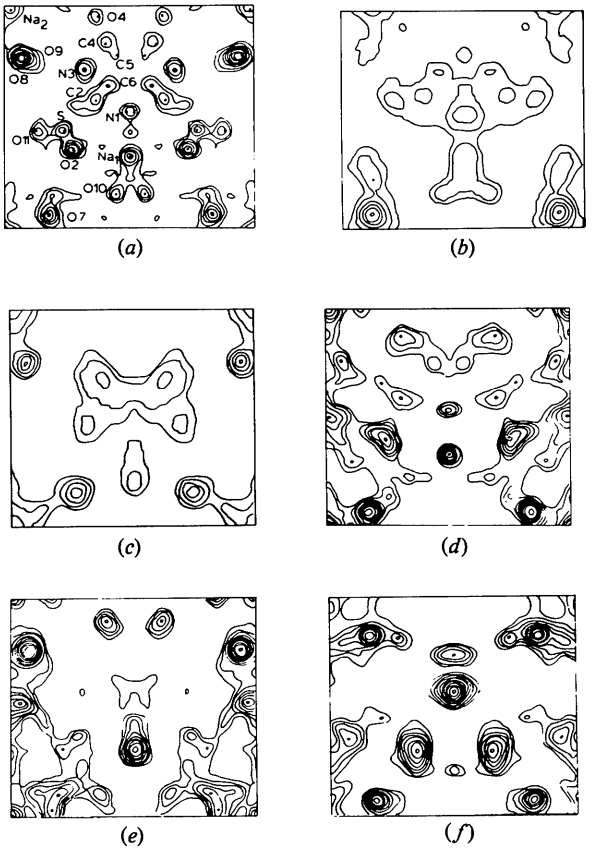

Fig. 4. Potential maps for DISOPS after direct phasing (half unit cell only). (*a*) Successful solution representative of 100 kV, 14 and 69 Å thicknesses; 1000 kV, 14 and 69 Å thicknesses, atom positions indicated. (*b*)–(*f*) Distorted potential maps respectively representative of: (*b*) 100 kV, 280 Å (No. 3); (*c*) 100 kV, 350 Å (No. 4); (*d*) 1000 kV, 280 Å (No. 7); (*e*) 1000 kV, 560 Å (No. 8); (*f*) 1000 kV, 690 Å (No. 9).

exact. However, for purposes of predicting the feasibility of a correct structure solution, the R value comparing kinematical and dynamical data might be thought to assess the validity of the crystal structure determined using the kinematic approximation for true 'experimental data' from a perfect single crystal. Testing this analogy to the conventional residual for a centric crystal with random placement of the proper atomic contents, the R value is predicted to be 0·83 (Wilson, 1950). R values within the range 0·4 to 0·5 are usually taken to indicate a centrosymmetric structure model which is somewhat correct (Stout & Jensen, 1968). Reference to Tables 1 and 4 reveals some conditions for which the R values alone would not anticipate the derivation of a correct structural model, again given the usefulness of this analogy of R's. Yet the maps reveal a clear representation of the molecule (*e.g.* cytosine data sets 2 and 6; DISOPS data set 2). Apparently, the most critical condition for the success of direct phasing is the distribution of high and low E values. Thus, dynamical effects may cause significant changes in $|F(\mathbf{h})|$, but if the patterns of large and small $|E_{\mathbf{h}}|$'s remain fairly consistent withal, direct phasing will succeed.

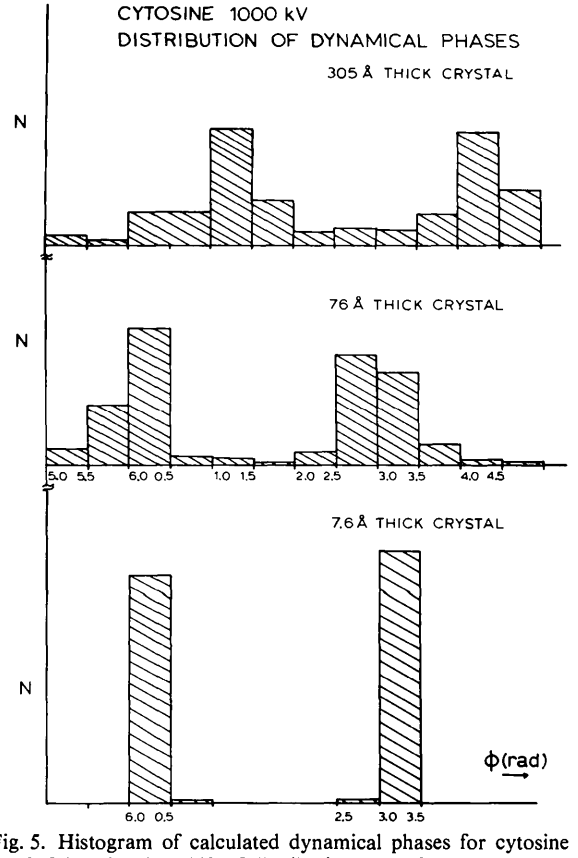

Fig. 5. Histogram of calculated dynamical phases for cytosine at 1000 kV showing shift of distribution away from 0, π at greater crystal thickness.

Calculation of molecular images from n-beam dynamical data

In a previous publication on direct phasing of electron diffraction data by Dorset & Hauptman (1976), it was suggested that the direct-method procedure (which allows the correct application of 'kinematical' phases to dynamical structure-factor moduli) might be more successful for deriving a molecular image than direct imaging in the electron microscope under ideal conditions (which uses both dynamical phases and diffracted-wave amplitudes). This suggestion stems in part from the observation that correct phases applied to scrambled values of X-ray structure-factor moduli nevertheless yield a recognizable representation of the crystal structure, even though the atomic weighting may be false (Ramachandran & Srinivasan, 1970). There is no doubt that the dynamical phases deviate significantly from their kinematical values. This is demonstrated in Fig. 5 for three cytosine data sets at 1000 kV. As the crystal thickness increases (and, hence, the importance of dynamical scattering), the distribution of phases shifts its maxima away from 0, π. As expected, the r.m.s. phase error increases also.

Dynamical images were calculated from the n-beam diffraction data to assess directly the confusion imparted to this visualization of the crystal structure. Intensity-modulated contour plots of images of the transmitted wave intensity, which were calculated at various crystal thicknesses, are shown in Figs. 6 and 7. The images show a gradual change as the specimen thickness increases, and at large crystal thickness corresponding to large values of the R factor, the images and the actual projected structure become very dissimilar. However, the degree of inaccuracy of the structure produced in the image is no worse than that produced by the direct phasing method, contrary to what may have been supposed. In fact, the correct interpretability of the transmitted wave (image) intensities produced at 1 MeV is superior to that of the maps obtained by direct phasing. Yet, these image calculations themselves are idealizations since they do not account for resolution limitations due to radiation damage (Glaeser, 1975) and instrument aberrations (Chiu, 1978).

Discussion

The derivation of real organic crystal structures from electron diffraction intensity data may be reliably executed by direct phasing methods, under suitable experimental conditions. The impositions of n-beam dynamical scattering effects will create little obstruction to direct phasing for reasonably thin perfect crystals.

The success of direct phasing is dependent upon the number of reflections with sufficiently large values of

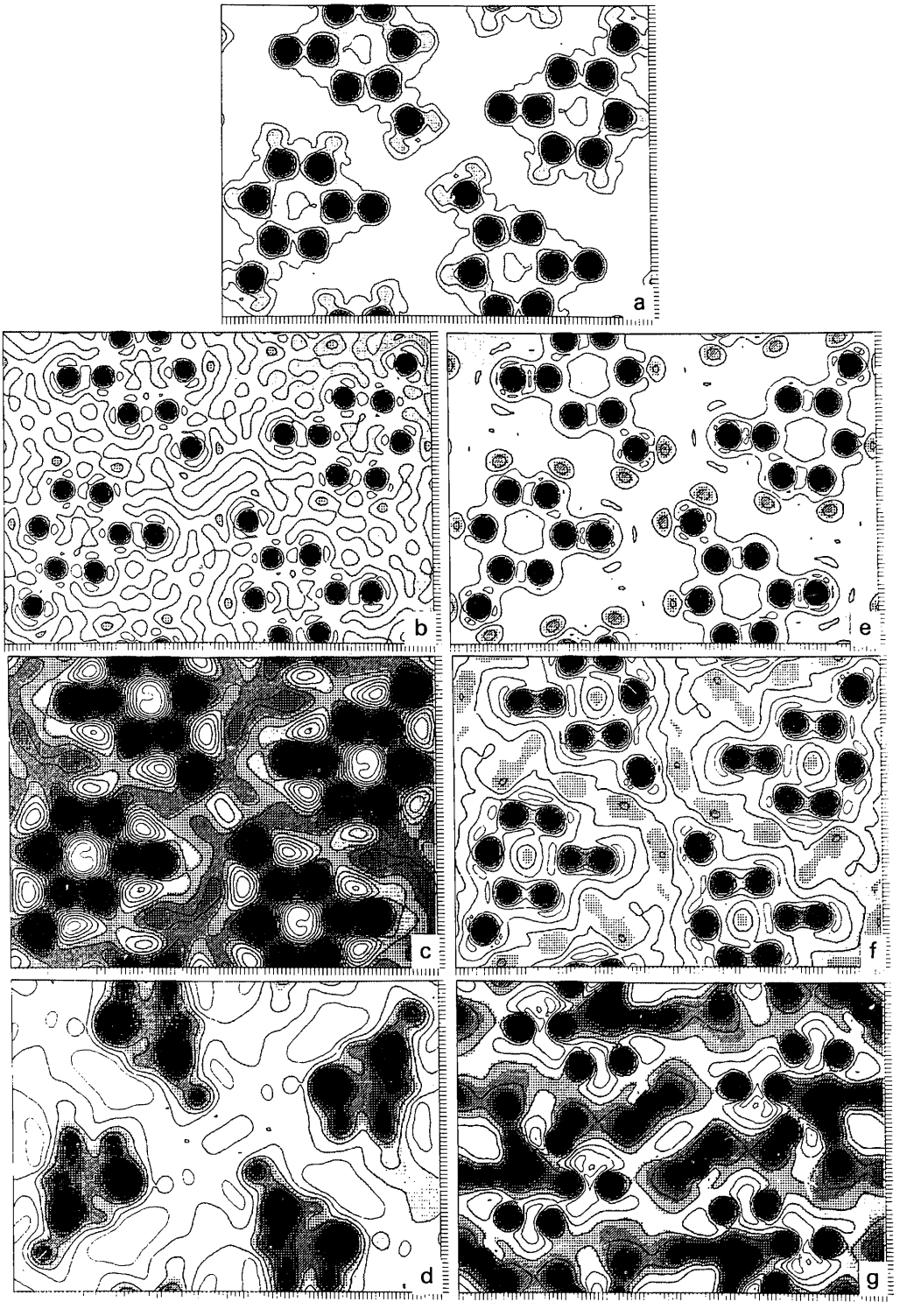

Fig. 6. Half-tone displays of the projected potential (*a*) and *n*-beam dynamical images of cytosine corresponding to data sets input to the direct phasing procedure (see Tables 1 and 4); (*b*)–(*d*) cytosine data sets 1–3; (*e*)–(*g*) cytosine data sets 5–7.

$|E|$ compared to the number of atoms in the asymmetric unit. For example, in the two paraffinic structures first investigated by this technique (Dorset & Hauptman, 1976), there were, respectively, 24 and 14 phased reflections per carbon atom. In the present study there are a minimum of eight phased reflections per heavy atom for cytosine and four phased reflections per heavy atom for DISOPS.

Organic molecular crystals rarely are perfect; they are particularly susceptible to bending (Dorset, 1978) and will thus be subject to further modulation of the diffraction intensities due to this imperfection (Cowley, 1961). For uniformly bent crystals with small unit-cell dimensions in the beam direction, there is some theoretical justification to believe that the wide-angle diffraction data will appear to emanate from thinner crystal layers than will the small-angle data; *i.e.* the higher-angle data will appear to be 'more kinematical' than the low-angle data. As pointed out by Cowley (1961) this is probably the reason that pioneering work (Vainshtein, 1964) in electron diffraction structure analysis used the kinematical theory with such success. On the other hand, the readily obtained $0kl$ zone-axis diffraction pattern of cytosine has considerably fewer reflections, to the same resolution, than are available in the $hk0$ orientation, and one cannot safely predict from the results presented here that the direct phasing method would be successful in the $0kl$ orientation.

Thus, the use of experimental data obtained from real (bent) crystals, for the purpose of a structure

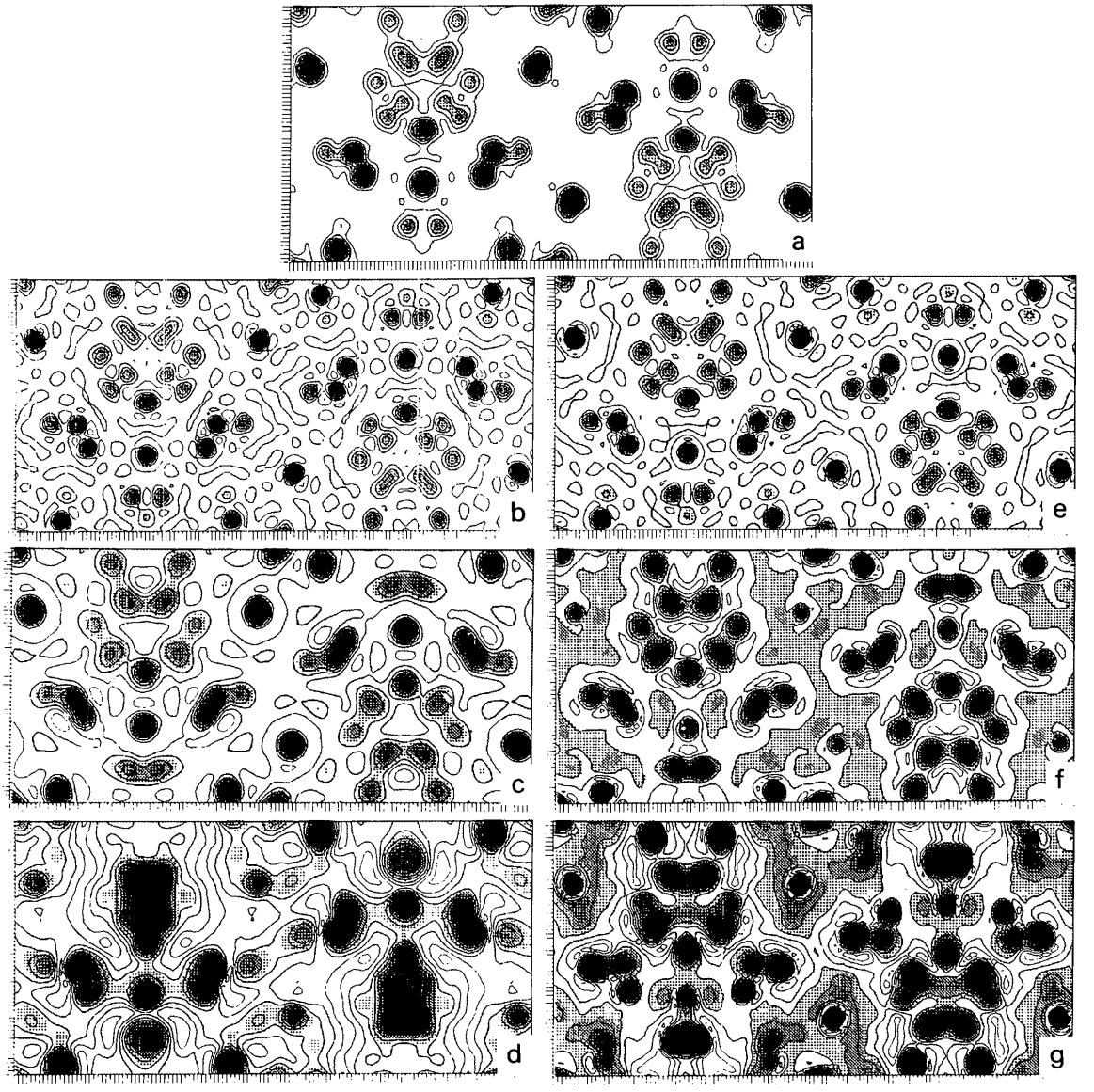

Fig. 7. Half-tone displays of projected potential (*a*) and *n*-beam dynamical images of DISOPS corresponding to data sets input to the direct phasing procedure (see Tables 1 and 4); (*b*)–(*d*) DISOPS data sets 1–3; (*e*)–(*g*) DISOPS data sets 6–8.

analysis by direct phasing must be done cautiously. The experimentally measured intensities will not only depend upon the diffraction conditions, excitation errors, *etc.*; the measured intensities will also depend greatly upon the relative areas (volumes) of the crystal that are bent to nearly satisfy one or another Bragg condition. Since single-crystal electron diffraction data are commonly collected from an area only a few micrometers in diameter, there can be relatively large statistical variations among the relative areas associated with bend contours of different Miller indices. For this reason alone the observed intensities in any one diffraction pattern of a bent crystal may bear no simple relationship whatsoever to either the kinematic or the dynamical intensities expected from an unbent crystal (see Cowley, 1961; Dorset, 1978). However, for structures with long unit-cell axes the conditions proposed in this model study, *i.e.* crystal orientations with the smallest unit-cell axis parallel to the incident beam, are those which minimize bending effects to diffracted intensities. Furthermore, as stated above, this crystallization can be imposed by epitaxy (for long-chain materials see also a review by Mauritz, Baer & Hopfinger, 1978).

With this caveat in mind, it is still useful to explore the possibilities of direct phasing on electron diffraction data from crystals for which atomic-resolution images are not obtainable. This paper represents an initial attempt to define the perturbation of this process due to dynamical scattering. Further work in this area is needed – *e.g.* to monitor diffraction from smaller slice-thickness intervals in domains where direct phasing is found to break down (for cytosine between 76 and 300 Å at 100 kV and between 300 and 610 Å at 1000 kV, for DISOPS between 69 and 280 Å for both voltages). Probably related to this particular study is the effect of diminished numbers of $|E|$'s > 1 for each atom of the asymmetric unit on the successful direct phasing of dynamical data. The use of more powerful higher-order invariant and seminvariant relationships will be investigated in this regard. Also, this paper did not deal with the prediction of an optimal accelerating voltage for use of electron diffraction data in the direct phasing procedure. As pointed out by Cowley (1975) for *n*-beam dynamical scattering, as the accelerating voltage of the incident electron beam increases (lower wavelength), an interaction constant for the scattering decreases. However, at higher electron energies the Ewald sphere also becomes flatter causing the excitation of more wide-angle beams (the excitation error approaches zero). Thus an optimal voltage for electron diffraction – and the success of direct phasing – probably lies between the two considered in this paper. Finally, an exhaustive study of bend effects on projections down long unit-cell axes is needed to assess the success of direct phasing on solution-grown microcrystals. These topics will be the subject of future work.

The work reported here has been supported in part by research grants from the NIH Nos. GM21047 and GM19452. The authors are grateful for helpful criticism of this work by Dr H. A. Hauptman.

References

BARKER, D. L. & MARSH, R. E. (1964). *Acta Cryst.* **17**, 1581–1587.

BOUDEULLE, M. (1975). *Cryst. Struct. Commun.* **4**, 9–12.

CHIU, W. (1978). *Scanning Electron Microscopy*, Vol. I, pp. 569–580. AMF O'Hare, SEM Inc.

COWLEY, J. M. (1961). *Acta Cryst.* **14**, 920–927.

COWLEY, J. M. (1975). *Diffraction Physics*, pp. 201–202. Amsterdam: North-Holland.

COWLEY, J. M. & MOODIE, A. F. (1957). *Acta Cryst.* **10**, 609–619.

DETITTA, G. T., EDMONDS, J. W., LANGS, D. A. & HAUPTMAN, H. (1975). *Acta Cryst.* A**31**, 472–479.

DORSET, D. L. (1977). *Z. Naturforsch. Teil A*, **32**, 1166–1172.

DORSET, D. L. (1978). *Z. Naturforsch. Teil A*, **33**, 964–982.

DORSET, D. L. & HAUPTMAN, H. A. (1976). *Ultramicroscopy*, **1**, 195–201.

DOYLE, P. A. & TURNER, P. S. (1968). *Acta Cryst.* A**24**, 390–397.

GLAESER, R. M. (1975). *Physical Aspects of Electron Microscopy and Microbeam Analysis*, edited by B. M. SIEGEL & D. R. BEAMAN, pp. 205–209. New York: Wiley.

HAUPTMAN, H. A. (1972). *Crystal Structure Determination: The Role of The Cosine Seminvariants*. New York: Plenum Press.

HEGER, G., KLEIN, S., PINTSCHOVIUS, L. & KAHLERT, H. (1978). *J. Solid State Chem.* **23**, 341–347.

JAP, B. K. & GLAESER, R. M. (1980). *Acta Cryst.* In the press.

JENSEN, L. H. (1970). *J. Polym. Sci. Part C*, No. 29, 47–63.

KARLE, I. L., DRAGONETTE, K. E. & BRENNER, S. A. (1965). *Acta Cryst.* **19**, 713–716.

KARLE, J. & KARLE, I. L. (1966). *Acta Cryst.* **21**, 849–859.

LANGS, D. A. & DETITTA, G. T. (1965). *Tenth International Congress of Crystallography*, Abstract 02.2.14.

MAURITZ, K. A., BAER, E. & HOPFINGER, A. J. (1978). *J. Polym. Sci. Macromol. Rev.* **13**, 1–61.

MURATA, Y., FRYER, J. R. & BAIRD, T. (1976). *J. Microsc. (Oxford)*, **108**, 261–275.

NOWACKI, W., MATSUMOTO, T. & EDENHARTER, A. (1967). *Acta Cryst.* **22**, 935–940.

RAMACHANDRAN, G. M. & SRINIVASAN, R. (1970). *Fourier Methods in Crystallography*, pp. 60–71. New York: Wiley.

SLETTIN, J. (1969). *J. Am. Chem. Soc.* **91**, 4545–4549.

STOUT, G. H. & JENSEN, L. H. (1968). *X-ray Structure Determination. A Practical Guide*, pp. 246, 327–328. New York: Macmillan.

UYEDA, N., KOBAYASHI, T., SUITO, E., HARADA, R. & WATANABE, M. (1972). *J. Appl. Phys.* **43**, 5181–5189.

VAINSHTEIN, B. K. (1964). *Structure Analysis by Electron Diffraction*, translated and edited by E. FEIGL & J. A. SPINK. Oxford: Pergamon Press.

WILSON, A. J. C. (1950). *Acta Cryst.* **3**, 397–398.